MEDICAL ROBOTS

Soft robotic ventricular assist device with septal bracing for therapy of heart failure

Christopher J. Payne,[1,2] Isaac Wamala,[3,4] Daniel Bautista-Salinas,[3] Mossab Saeed,[3] David Van Story,[1,2,3] Thomas Thalhofer,[1,2,5] Markus A. Horvath,[1,2,6] Colette Abah,[1,2] Pedro J. del Nido,[3] Conor J. Walsh,[1,2]* Nikolay V. Vasilyev[3]*

Previous soft robotic ventricular assist devices have generally targeted biventricular heart failure and have not engaged the interventricular septum that plays a critical role in blood ejection from the ventricle. We propose implantable soft robotic devices to augment cardiac function in isolated left or right heart failure by applying rhythmic loading to either ventricle. Our devices anchor to the interventricular septum and apply forces to the free wall of the ventricle to cause approximation of the septum and free wall in systole and assist with recoil in diastole. Physiological sensing of the native hemodynamics enables organ-in-the-loop control of these robotic implants for fully autonomous augmentation of heart function. The devices are implanted on the beating heart under echocardiography guidance. We demonstrate the concept on both the right and the left ventricles through in vivo studies in a porcine model. Different heart failure models were used to demonstrate device function across a spectrum of hemodynamic conditions associated with right and left heart failure. These acute in vivo studies demonstrate recovery of blood flow and pressure from the baseline heart failure conditions. Significant reductions in diastolic ventricle pressure were also observed, demonstrating improved filling of the ventricles during diastole, which enables sustainable cardiac output.

INTRODUCTION

Soft robots fabricated from low-modulus materials with the ability to conform to their environment have gained notable interest in recent years (*1*–*6*). The inherent compliance of these robots means that they can be configured to perform complex biomimetic motions that cannot be achieved by conventional rigid robots (*7*–*11*). The emergence of this technology has made a compelling alternative to rigid devices in many biomedical applications, such as soft interventional instrumentation (*12*–*14*). Soft robotic technologies are also ideally suited to smart wearable devices that synergistically interact with the human wearer to provide assistance or rehabilitation. Examples of this approach include assistive soft robotic gloves (*15*, *16*), soft exosuits for walking assistance (*17*–*19*), and devices for soft tissue manipulation (*20*). Recently, soft robotic devices have been proposed to support the heart in failure. These designs exploit conformable soft actuators that assist the native heart muscles (*21*–*25*) or provide a means to pump blood directly (*26*).

Heart failure (HF) is a condition in which the heart cannot generate sufficient blood flow to meet the metabolic needs of the body. Prevalence of HF in the United States is around 5.7 million, with a total financial cost to the economy of $30.7 billion a year (*27*). HF can occur in the left ventricle (LV) or the right ventricle (RV) or in both ventricles and can be caused by a diverse range of congenital and acquired diseases. Heart or heart-lung transplantation is a widely accepted therapy for end-stage HF, but the availability of donor organs is limited (https://optn.transplant.hrsa.gov/), and many patients are ineligible for transplant surgery. Ventricular assist devices (VADs) are an accepted therapeutic solution when a donor organ is not available. VADs are used as a bridge to recovery that allows a heart muscle to recover from an acute injury, as a bridge to transplant, or for permanent implantation. Most VADs in current clinical practice are extracardiac and intracardiac pumps that unload the heart by diverting blood flow from the diseased ventricle through an artificial circuit connected to the heart chambers or the vasculature. Most of the latest VADs use impellers to provide continuous blood flow through a lumen (*28*–*30*). A major problem with these designs is the risk of thrombi formation resulting from interaction between the flowing blood and nonbiologic components within the lumen of the device. Thrombus formation and thromboembolic events are still common with VADs and are associated with high morbidity and mortality (*31*). Patients with an implanted VAD must undergo permanent anticoagulation therapy; such therapy increases the risk of bleeding, both at the site of VAD implantation and within the internal organs (*32*).

Alternative therapeutic options for end-stage HF have been used, including stem cell therapies, passive restraining devices, and direct cardiac compression devices (*33*–*36*). Although the use of stem cells and biological agents for cardiac regeneration has shown promising results in both animal studies and clinical trials, remaining challenges include engraftment, mobilization, and poor survival of stem cells (*33*, *37*). Passive ventricular restraint devices have mostly targeted HF in the LV, and the long-term benefits for such an approach remain to be studied (*35*). RV restraint, with or without simultaneous involvement of the LV, has been studied in experimental settings, showing moderate improvements in ejection fraction (*38*).

Direct cardiac compression devices placed around the heart can augment blood ejection in systole without contacting the blood (*36*). The majority of these devices use a pneumatic cuff to compress the ventricles, which can invert the natural shape of the heart. To address this issue, a soft robotic sleeve that mimics the natural motion

[1]Wyss Institute for Biologically Inspired Engineering, 3 Blackfan Circle, Longwood, Boston, MA 02115, USA. [2]Harvard John A. Paulson School of Engineering and Applied Sciences, Harvard University, 29 Oxford Street, Cambridge, MA 02138, USA. [3]Department of Cardiac Surgery, Boston Children's Hospital, 300 Longwood Avenue, Boston, MA 02115, USA. [4]Department of Cardiovascular Surgery, Deutsches Herzzentrum Berlin, Berlin, Germany. [5]Department of Mechanical Engineering, Technical University of Munich, Munich, Germany. [6]Harvard-MIT Health Sciences and Technology, Massachusetts Institute of Technology, 77 Massachusetts Avenue, Cambridge, MA 02139, USA.
*Corresponding author. Email: nikolay.vasilyev@childrens.harvard.edu (N.V.V.); walsh@seas.harvard.edu (C.J.W.)

of the heart was proposed and shown to restore aortic blood flow in an acute HF model (*21*). Direct compression devices have the advantage of not contacting blood, but they cannot engage the interventricular septum (IVS). Isolated HF in the RV or LV can also cause abnormal bowing of the IVS toward the opposite ventricle as blood pressure in the diseased ventricle increases because of congestion (*39*–*41*). This distortion of the IVS cannot be corrected with direct cardiac compression devices and can even be exacerbated after implantation of traditional VADs (*42*). To augment septal motion in HF, a contractile actuator that can be fully implanted inside the RV has been proposed to cause approximation of the RV free wall and the septum during ventricular contraction (*25*). However, the cardiac augmentation performance of this approach is limited by the contractile range of the actuator and by the fact that the force can only be applied at a single point on the ventricular free wall. The limited actuator range is a drawback given the contribution of the IVS to blood ejection, especially in the RV, in which septal contraction plays a critical role (*39*, *43*). Furthermore, direct cardiac compression devices cannot correct mechanical desynchronization between the contraction of the ventricular free wall and the septum.

Here, we propose a soft robotic VAD that is anchored to the ventricular free wall and the IVS. An anchoring system, a bracing structure, and soft actuators are configured so that compressive forces are externally applied to the ventricular free wall while the reaction forces are transmitted to the IVS during systole. This process enables the ejection of additional blood volume from the target ventricle (Fig. 1, A to C, and movie S1). The device actively recoils the ventricular free wall during diastole, which assists with ventricular diastolic refilling. The soft robotic VAD is implanted onto the beating heart under three-dimensional echocardiography guidance; this avoids the need for open-heart surgery and the use of cardiopulmonary bypass that can lead to neurological complications (*44*). In this work, we demonstrate effective engagement of the septum in a soft robotic VAD concept that can restore function of both the RV and the LV. We present the device concept, actuator characterization, ex vivo validation, and in vivo studies. When implanted on either the RV or the LV, the devices can effectively recover heart function in a range of HF models that represent differing HF conditions.

RESULTS

The soft robotic VADs use a combination of soft actuators and a bracing assembly to apply rhythmic loading to the ventricle wall, with the reaction forces transmitted to the IVS (Fig. 1, A to C, and movie S1). The bracing assembly consists of a septal anchoring mechanism, a bracing bar with a sealing sleeve that passes through a ventricle wall, and a semilunar bracing frame that is mounted around the ventricle (Fig. 1D). The semilunar bracing frame incorporates embedded soft actuators based on the McKibben pneumatic artificial muscle design that provide external compression to the outer surface of the ventricle free wall. The actuators incorporate an elastic bladder and mesh braid to provide contractile motion when inflated. The actuators are constrained in a curved configuration within the semilunar frame so as to straighten and radially expand when actuated. During the diastolic phase of the cardiac cycle, the actuators recoil back to the curved configuration within the semilunar frame (Fig. 1, A and B). When mounted in the semilunar frame, these actuators can generate linear displacements of 20 to 40 mm (fig. S1) at response times under 200 ms (fig. S2). Force characterization experiments demonstrate that loads exceeding 100 N can be delivered from the actuators in the proposed design configuration (fig. S3). A full description of these characterization studies is provided in the Supplementary Materials.

Separate implementations of the soft robotic VAD concept were fabricated for use on the RV and the LV to account for the distinctly contrasting anatomy and mechanics of each ventricle; this design choice was determined through ex vivo testing. The LV wall is thick

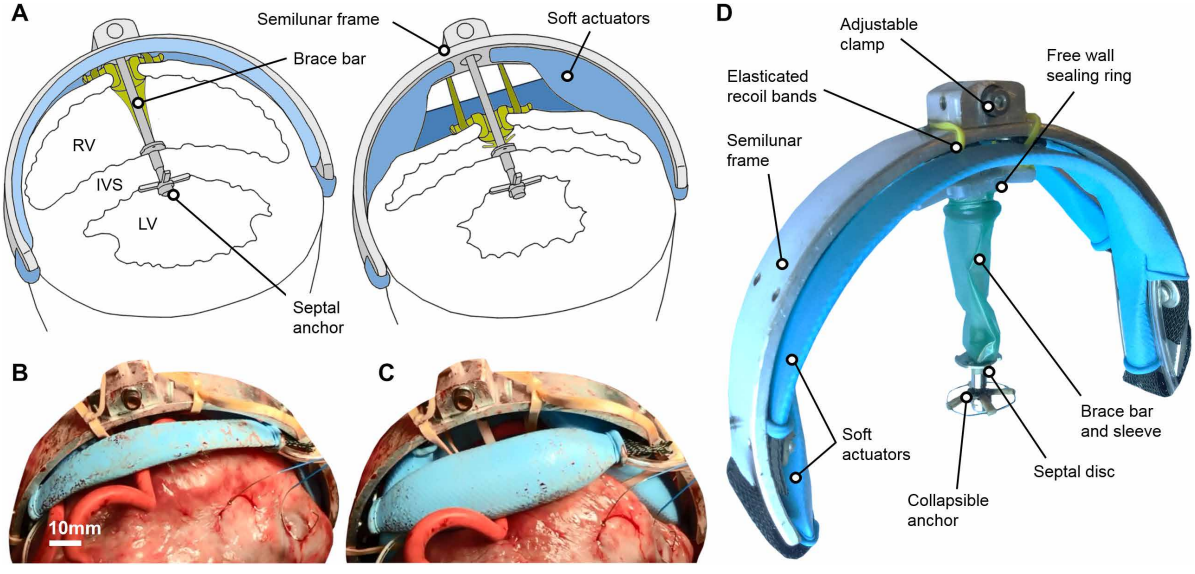

Fig. 1. Soft robotic VAD concept. (**A**) Section view illustration showing the soft robotic device principle of operation on the right side of the heart in diastole (left) and systole (right; outermost central actuator is removed here for illustrative purposes). (**B**) Photograph of the soft robotic device during in vivo operation on the RV in diastole (the red object is the standard surgical tourniquet used to tension the purse string suture that retains the sealing ring in the ventricle wall). (**C**) Photograph of the device on the RV in systole. (**D**) Annotated photograph of the device implementation for the RV.

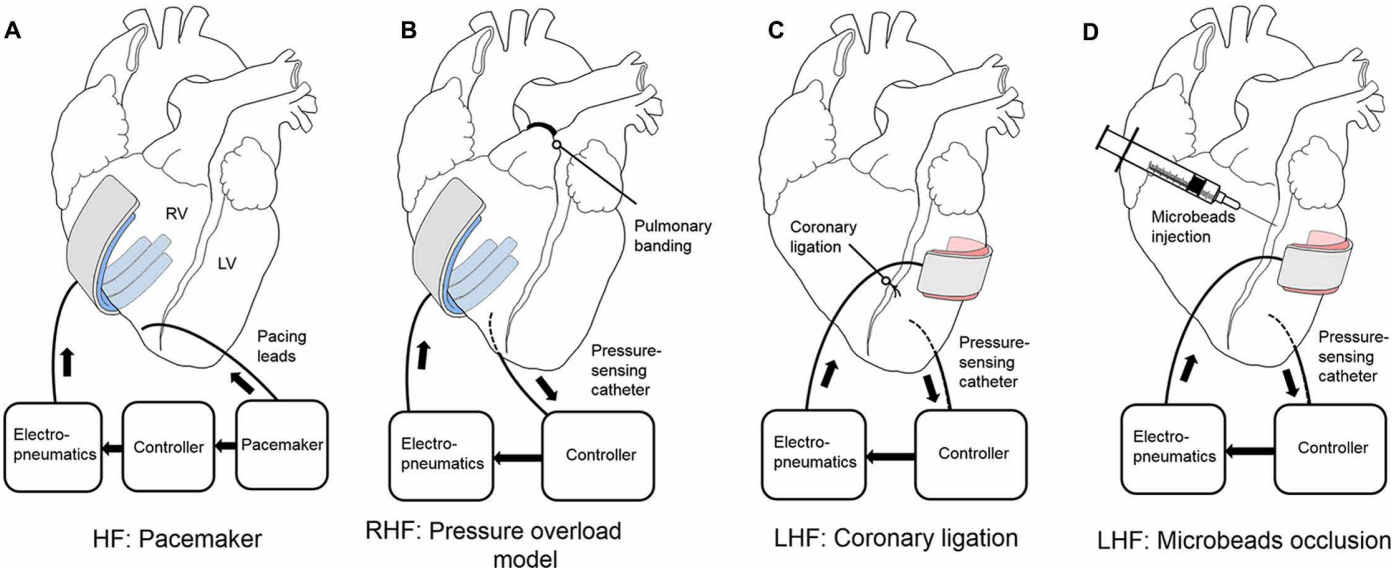

Fig. 2. Soft robotic VAD implementations, control schemes, and HF models. (**A**) Soft robotic device as applied to the RV with pacing for control and as a HF model. (**B**) Device applied to the RV with pressure-triggering control and a pressure overload RHF model. (**C**) Soft robotic device applied to the LV with coronary ligation LHF model. (**D**) Soft robotic device applied to the LV with a coronary microvasculature occlusion LHF model.

(~20 to 30 mm) and approximately conical profiled. Conversely, the RV wall is much thinner (~5 to 8 mm) and is a crescent-shaped structure that is wrapped around the LV (*45*, *46*). The soft robotic device implementation for the RV incorporates a semilunar frame of 200° arc angle and is oriented along the length of the RV, spanning from the heart apex to the distal region of the outflow tract (see Fig. 2, A and B). We incorporate four soft actuators within the semilunar frame. Two actuators are mounted centrally adjacent to the brace bar, and the other two actuators are mounted distally on either side of the brace bar (Fig. 1D shows the RV soft robotic device). The four actuators provide compression of a large region of the RV free wall in systole to maximize systolic ejection fraction. Furthermore, the RV is a relatively compliant structure; when a diseased RV is externally compressed, localized distention can occur to accommodate the increased blood pressure. This "ballooning" effect on the RV reduces the amount of blood that is ejected through the pulmonary artery and reduces the efficacy of external loading. The use of multiple actuators thus helps to constrain the RV in systole to maximize blood ejection. For the LV soft robotic device, the semilunar frame is smaller (150° arc angle). The device is positioned to be parallel with the heart base to accommodate the conical profile of the LV (Fig. 2, C and D). In this orientation, only two central actuators are required to provide effective compression of the LV free wall toward the septum. Because the LV free wall is thicker and comparatively stiffer compared with the RV, it is less prone to distention when externally loaded at a localized point.

A sealing ring is implanted within the free wall of the ventricle to allow unrestricted linear translation over the implanted bracing bar (Fig. 1, A and D). A thermoplastic sleeve is used to create a seal between the ring and the bracing bar to prevent bleeding from the access point in the free ventricle wall. To recoil the free ventricular wall and assist refilling during diastole, we used elasticated bands to couple the sealing ring and outer bracing frame (Fig. 1D). Alternatively, the soft actuators can be directly attached to the ventricle wall to assist distention of the ventricle in diastole. The device is implanted on the beating heart (Fig. 3, A to F); the deployment process is described in detail in Materials and Methods. Movie S2 illustrates the deployment process with corresponding echocardiography images.

Ex vivo soft robotic VAD testing

Ex vivo testing was performed to validate and optimize the design concept before in vivo testing (see the Supplementary Materials). Experiments were performed on instrumented porcine hearts to test both the RV and the LV devices. Hearts were pressurized with water, and the devices were implanted (Fig. 4A shows the LV experimental setup). The device actuators were cyclically inflated to 12 psi at 50 beats per minute (bpm). Both RV and LV devices could displace physiological volumes of water when actuating against a range of afterloads. The LV device could generate around 12 ml per cycle against afterload pressures of 40 to 100 mmHg (Fig. 4, B and C), and the RV device could produce around 20 ml per cycle against afterload pressures of 20 to 50 mmHg (fig. S4). In both cases, the volume of fluid displaced during device operation was observed to be relatively independent of afterload pressure.

The two–actuator device embodiment was originally assessed on the RV (movie S1) before the additional distal actuators were incorporated into the design. Experimentation confirmed that greater flow rate and peak pressures can be achieved with all actuators (Fig. 4, D to G). We also recorded the motion of the septal anchoring system during device actuation using an endoscope inserted inside the RV (movie S3).

Preliminary RV device characterization using a pacing HF model

Initial characterization of the RV device was assessed through an in vivo porcine study. We used pacing of the RV to disrupt the native heart rhythm and cause acute HF (Fig. 2A). The pacemaker signal was also used as a control input to trigger contraction of the soft actuators in synchrony with the heart. Measurements of blood pressure and flow were taken under baseline conditions, in HF, and during device actuation under various operating conditions. We assessed

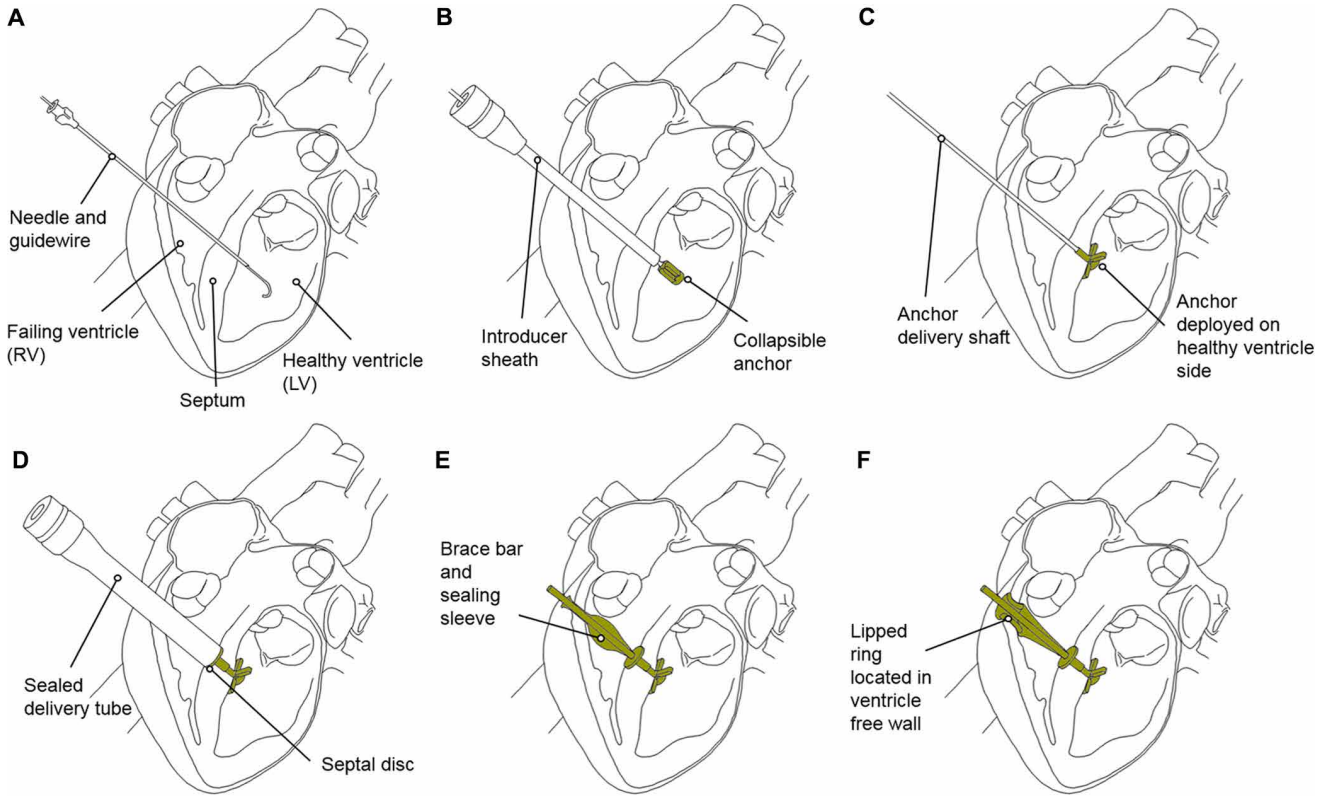

Fig. 3. Deployment of the septal anchoring system. (**A**) Insertion of needle and guidewire under ultrasound guidance. (**B**) Insertion of a 20-French introducer sheath and deployment of a collapsible septal anchor. (**C**) Removal of the introducer sheath and retraction of the deployed septal anchor. (**D**) Introduction of a delivery tube and coupling of a tip-mounted septal disc to a collapsible anchor. (**E**) Coupling of a bracing bar and removal of the delivery tube. (**F**) Insertion of the ventricle wall sealing ring. Implanted components are shown in green.

the force exerted on the RV by the soft robotic device (Fig. 5, A to C) using a modified semilunar bracing frame with integrated force sensors to quantify the total axial force transmitted to the septum during device operation. Peak force measurements of 14 to 18 N were observed at actuator inflation pressures of 10 psi (Fig. 5B). We also observed that increased actuator inflation pressures only resulted in modest improvements to pulmonary flow rate but resulted in significantly greater load being applied to the RV free wall (fig. S5).

We studied the effect of altering actuation timing conditions on pulmonary flow output to achieve optimal synchronization between the heart and the device. We varied both systolic actuation period (defined as a percentage fraction of the total cardiac cycle) and the time delay after the initial pacemaker signal. The device was actuated during HF for all combinations of systolic periods (25, 30, 35, and 40% of the cardiac cycle period) and delay periods of 0, 5, and 10% of the total cardiac cycle period (Fig. 5D). The systolic actuation period was shown to be a more significant factor for maximizing pulmonary flow than the delay period, with 35% being the optimum period for a 96-bpm heart rate. The results indicate that the device is tolerant to timing delay discrepancies of up to 5% of the cardiac cycle at 96 bpm and 35% systolic actuation period. Otherwise, the addition of delays into the control system resulted in a loss of pulmonary flow output.

We studied the contribution of the different actuator pairings and use of the recoiling bands. As per the ex vivo study findings, in vivo testing demonstrated that all four actuators are necessary for optimum performance on the RV (Fig. 5E), although the central actuators provided the greatest contribution when the recoil bands were present. Under all actuation conditions, the elastic recoil bands enhanced pulmonary flow rate by distending the ventricle free wall to augment refilling. The soft robotic device was assessed in a steady state after 5 min of continuous operation (fig. S6, A to G). Overall, the device could significantly augment pulmonary flow to 66% of the healthy baseline from a HF baseline of 19%. End-tidal CO_2 represents the maximal concentration of carbon dioxide at the end of exhalation and is directly related to pulmonary blood flow. End-tidal CO_2 was markedly improved after actuation of the device (fig. S6C). Additional data showing augmentation of aortic flow and RV pressure are reported in the Supplementary Materials.

RV device performance in a right heart failure model resulting from pressure overload

HF in the RV often occurs as a result of pressure overload, a condition whereby elevated pressure inside the pulmonary artery increases the pumping burden of the RV. To simulate this right heart failure (RHF) condition, we placed an inextensible band around the main pulmonary artery to impede blood outflow from the RV and increase RV pressure (Fig. 2B). After banding, the pulmonary flow was reduced to 52% of baseline ($P < 0.001$). To synchronize the soft robotic VAD with the native RV contraction, we introduced a pressure-sensing catheter (Scisense, Transonics Systems Inc.) into the RV and used it to trigger the device to actuate at the end of RV diastole. The soft

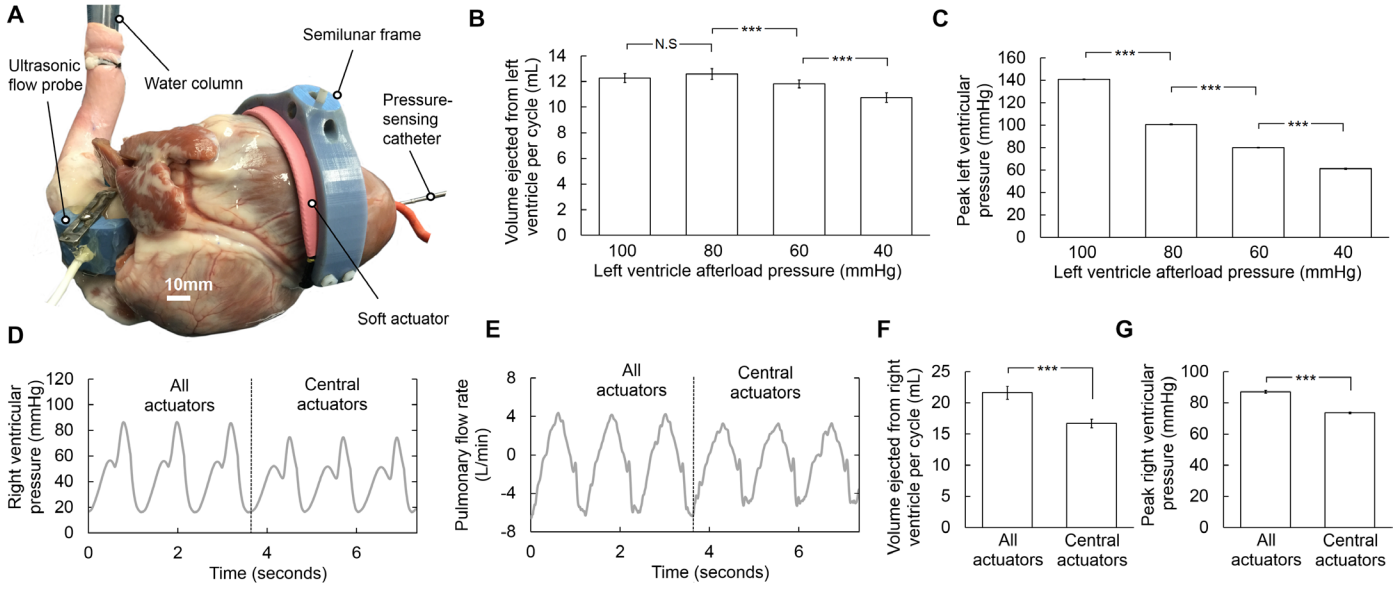

Fig. 4. Ex vivo testing of the soft robotic devices. (**A**) Experimental setup with instrumented heart (photograph shows device implementation for the LV). (**B** and **C**) Plots showing average volumetric ejection and peak pressures on the LV at a range of afterloads. NS, not significant. (**D** to **G**) Plots showing the pressure, flow rate, average volumetric ejections, and peak pressures for the device as applied to the RV. Error bars denote ±SD. ***$P < 0.001$.

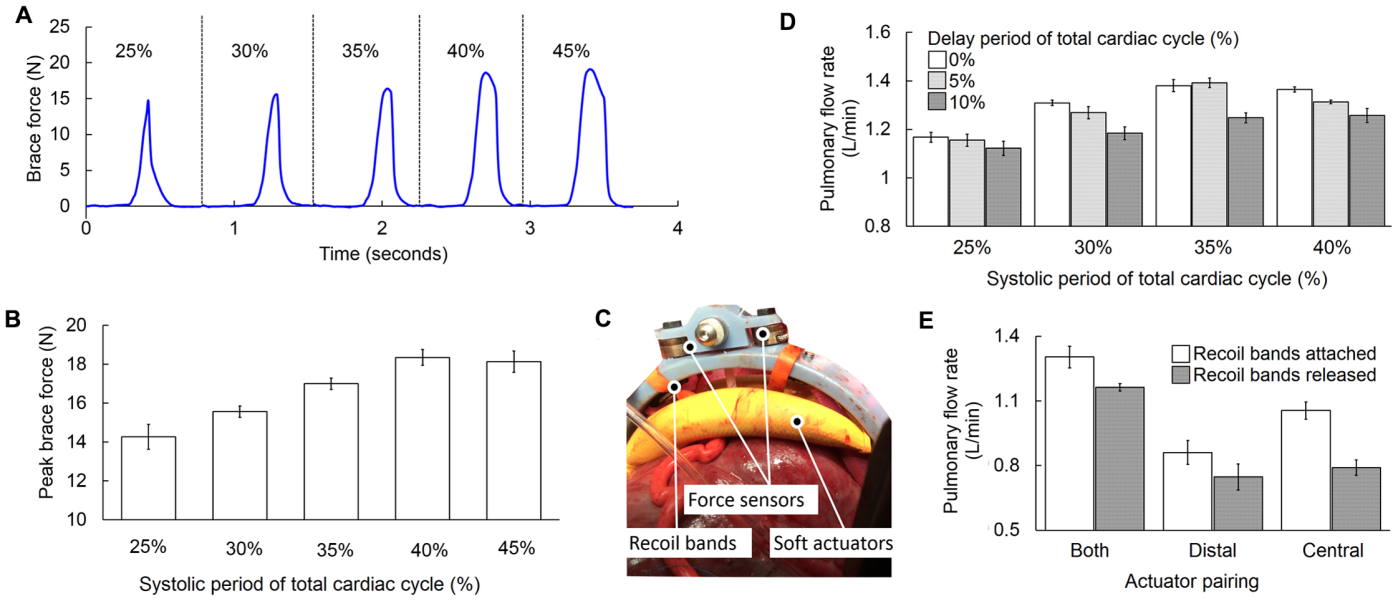

Fig. 5. In vivo characterization of the soft robotic device concept applied to the RV. (**A**) Brace force profiles for different systolic timings (as a percentage of total cardiac cycle) at an actuator inflation pressure of 10 psi. (**B**) Peak brace forces observed for different systolic actuation periods at an inflation pressure of 10 psi. (**C**) Photograph showing in vivo deployment of the device with integrated force sensors. (**D**) Characterization of pulmonary flow output for actuation of the device at different systolic actuation and delay periods. (**E**) Plot showing the contribution of actuator pairings on pulmonary flow rate. Error bars denote ±SD.

robotic controller was programmed to maintain the systolic contraction period at 35% of the cardiac cycle according to the instantaneous heart rate, which fluctuated from 98 to 105 bpm over the course of the study. We actuated the device continuously for a total of 50 min; pulmonary flow was maintained at 104% of the healthy baseline level ($P < 0.001$) (Fig. 6, A and D). Restoration of RV function also provided blood flow to the LV, leading to the restoration of aortic flow (Fig. 6, B and E). There was also a significant increase in peak RV pressure ($P < 0.001$) and a drop in end diastolic RV pressure ($P < 0.001$) after continuous device operation (Fig. 6, C, F, and G).

LV device performance in left heart failure models

To validate the LV device, we performed two in vivo porcine studies using models of left heart failure (LHF). In the first study, a coronary

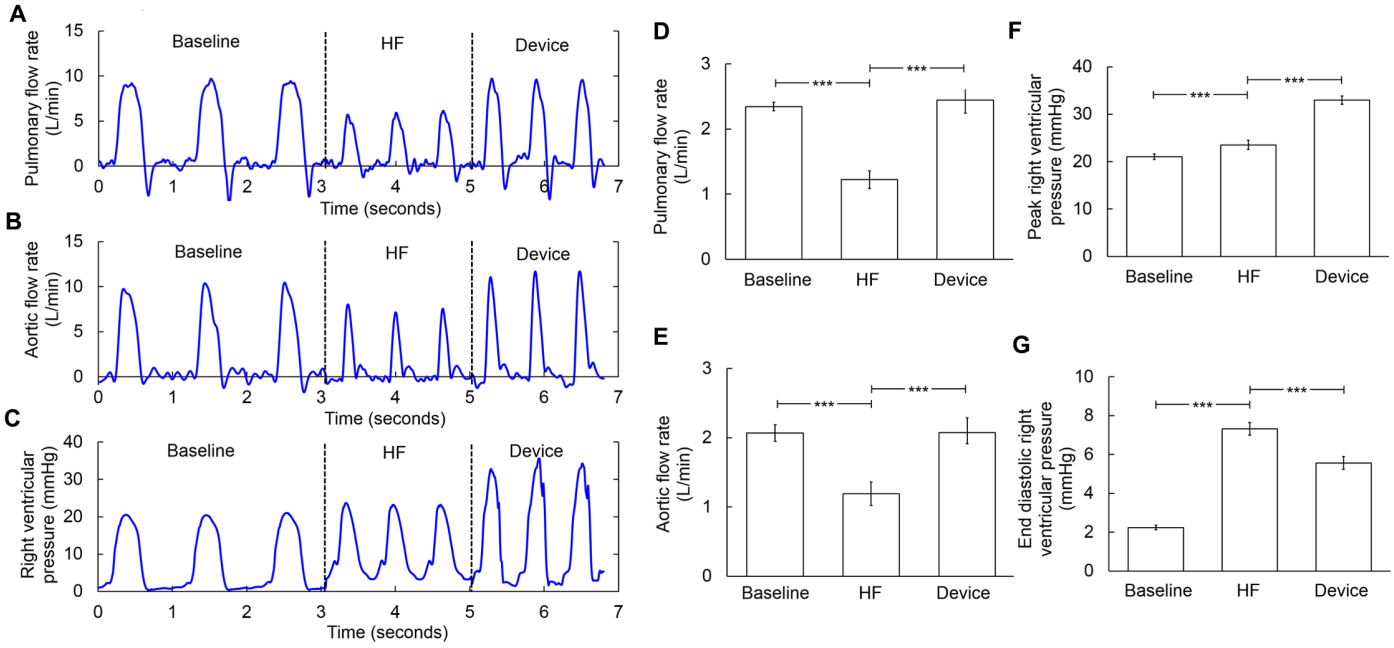

Fig. 6. Soft robotic device applied to the RV in a pressure overload model of RHF. (**A** to **C**) Plots showing pulmonary flow rate, aortic flow rate, and peak RV pressure versus time at baseline, at HF, and with the device actuating after 50 min of continuous operation. (**D** to **G**) Plots showing pulmonary flow rate, aortic flow rate, peak RV pressure, and end diastolic RV pressure at baseline, at HF, and with the device actuating after 50 min of continuous operation, for 15 consecutive cycles. Error bars denote ±SD. ***$P < 0.001$.

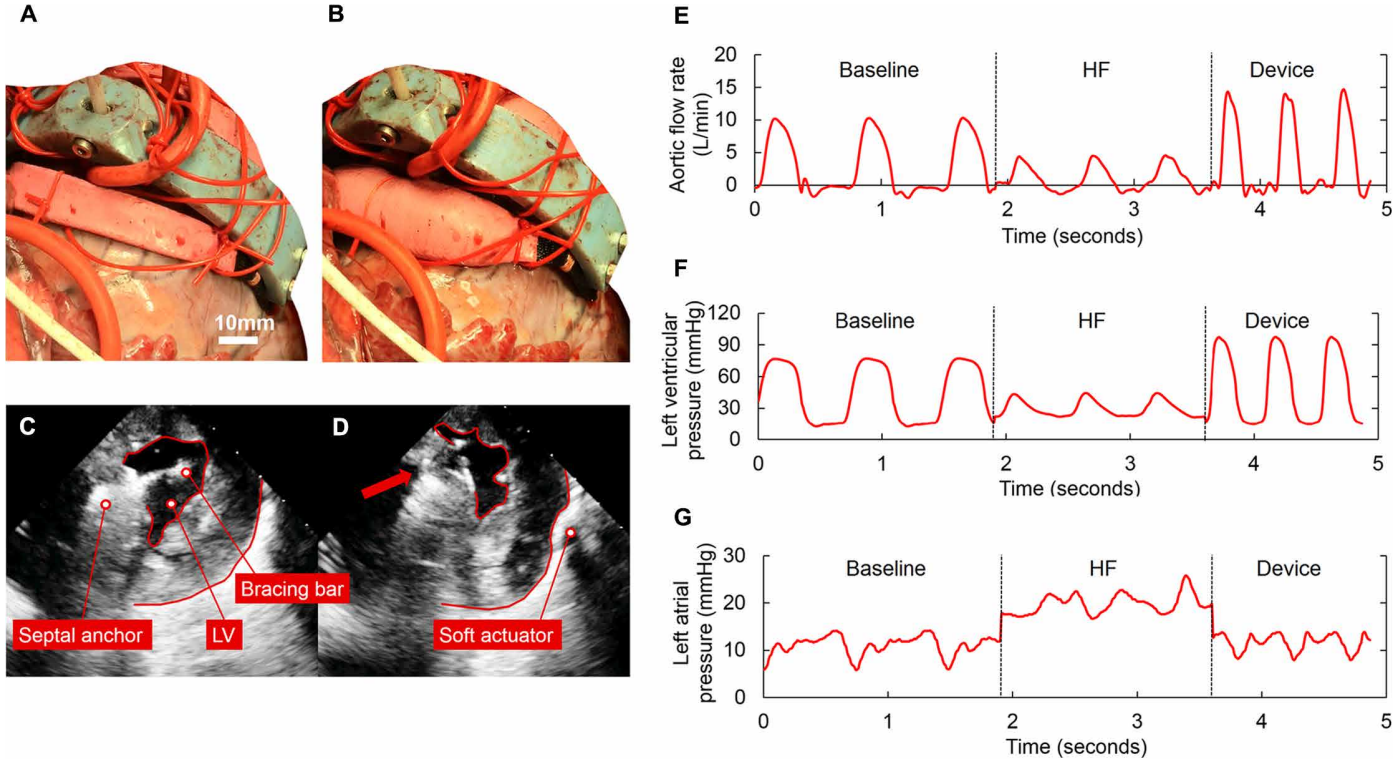

Fig. 7. Soft robotic device applied to the left side in a coronary ligation HF model. Photographs of the device in diastole (**A**) and in systole (**B**). Ultrasound images of the septal anchor and brace bar assembly in vivo: (**C**) the device in diastole and (**D**) the device in systole. (**E** to **G**) Aortic flow, LV, and LA pressure profiles of the LV device at baseline, at HF, and with the device actuating after 5 min of continuous operation.

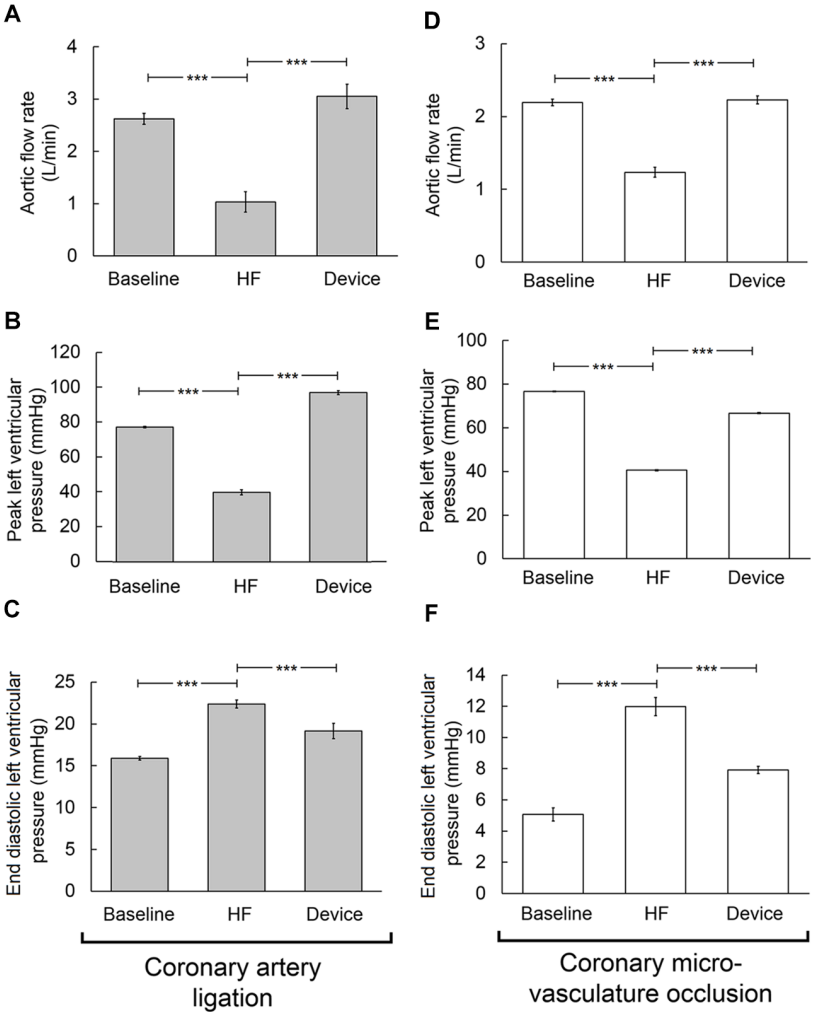

Fig. 8. Steady-state performance of the soft robotic device in LHF models. (**A** to **C**) Plots showing aortic flow rate, peak LV pressure, and end diastolic LV pressure at baseline, at HF, and with the device actuating after 5 min of continuous operation in a coronary artery ligation model of LHF. (**D** to **F**) Plots showing aortic flow rate, peak LV pressure, and end diastolic LV pressure at baseline, at HF, and with the device actuating after 50 min of continuous operation in a coronary microvasculature occlusion model of LHF. Data are based on 15 consecutive cycles. Error bars denote ±SD. ***$P < 0.001$.

artery ligation procedure was performed to cause ischemia selectively of the LV free wall and reduce LV contractility (Fig. 2C). After ligation, the aortic flow rate was reduced to 39% of the healthy baseline ($P < 0.001$). The LV soft robotic device was actuated, and cardiac output was assessed after 5 min of operation to negate transient effects (Fig. 7, A to G). In this experiment, we used the pressure-triggering methodology to synchronize the device with the native heart. The heart rate was 110 bpm during device operation (up from 81.5 bpm) under healthy baseline conditions. Aortic flow was significantly augmented from the HF condition ($P < 0.001$) and restored to 116% of the healthy baseline (Fig. 8A). Similarly, peak LV pressure was augmented from the LHF condition to the healthy baseline level (Fig. 8B). Both the mean left atrial (LA) pressure and end diastolic LV pressure dropped during actuation, indicating improved diastolic function of the LV (Figs. 7G and 8C, respectively). Echocardiography imaging of the heart was performed during device operation to visually assess the rhythmic loading of the septum (Fig. 7, C and D, and movie S3).

To demonstrate longer-term validation of the device on the LV, we used a coronary occlusion LHF model in an additional porcine study. We injected polystyrene microbeads with diameters ranging from 50 to 100 μm (Megabead NIST, Polysciences Inc.) into the coronary arteries to occlude the microvasculature of both LV free wall and the IVS (Fig. 2D). After the microbeads were injected, aortic flow was reduced to 56% of the healthy baseline ($P < 0.001$) (Fig. 8D). There was a corresponding drop in LV peak pressure ($P < 0.001$) and an increase in LV end diastolic pressure ($P < 0.001$) (Fig. 8, E and F). The device was implanted and actuated for a period of 50 min; the actuator contraction period was regulated at 40% of the cardiac cycle according to the instantaneous heart rate, which fluctuated from 83 to 93 bpm over the experiment duration. Heart function was recovered for this 50-min period of testing, with aortic flow returned to baseline levels ($P < 0.001$) and LV peak and end diastolic pressures both significantly improved.

DISCUSSION

We report a soft robotic VAD implant that augments cardiac function by bracing to the IVS and provides rhythmic loading to a target failing ventricle. The versatility of this approach has been demonstrated through in vivo studies on both ventricles across a diverse range of HF conditions including pressure overload RHF and ischemic LHF. Existing VAD designs do not engage the IVS, a critical structure within the heart that contributes significantly to blood ejection from the ventricles (*39*). The incorporation of septal bracing has demonstrated effective approximation of the ventricle free wall and the IVS in ex vivo and in vivo experiments. The use of a septal anchoring brace could also prevent bellowing of the septum toward the opposite ventricle in severely dilated hearts and correct desynchrony between the ventricle free wall and the IVS that can occur in HF.

The ability of the ventricle to refill with blood in between contractions is crucial for sustaining cardiac output. The provision of diastolic function augmentation has been a major shortcoming of previous VADs. In this work, significant improvements were observed in cardiac diastolic function for both ventricles in different HF modes. Diastolic dysfunction is characterized by raised filling pressures as the heart becomes congested. In this series of studies, device operation demonstrated marked improvements in both end diastolic LV pressure and mean LA pressure in the LHF experiments. Significantly reduced end diastolic RV filling pressures were observed in a pressure overload RHF model. Furthermore, the device did not adversely affect the LV during operation on the RV but instead facilitated augmentation of aortic flow.

Synchronization of the device with the native heart function was achieved using a pressure-sensing catheter placed inside the ventricle, which triggered device actuation at the end of diastole. The controller could also regulate the contraction timing of the actuators to be maintained at a fixed ratio of the cardiac cycle. This organ-in-the-loop control and real-time adjustment of the device timing parameters enabled fully autonomous augmentation of cardiac function. In both

RV and LV implementations, this control methodology proved robust to natural fluctuations in heart rate (up to 10 bpm change in both cases), allowing sustained periods of autonomous operation. We demonstrate the importance of setting the correct timing parameters for synchronizing such a device with the native heart contraction.

The incorporation of elasticated bands for recoiling the ventricle free wall during diastole demonstrated improved cardiac output. These results underscore the importance of mechanical coupling between cardiac compression VADs and the ventricle outer wall. The integration of force sensors into the bracing structure has also enabled real-time monitoring and quantification of the compression forces required to augment cardiac function in vivo. These data will guide the design of future soft robotic VADs and may facilitate the development of force control schemes for optimizing device performance in future work.

We have previously reported an intracardiac soft robotic device for RV augmentation (*25*). The device was based on a single McKibben actuator positioned inside the RV perpendicular between the free wall and septum. Device actuation resulted in an 8% increase of RV blood flow in an animal model of end-stage RHF where no native RV ejection was present. The current approach can generate significantly greater free wall to septum approximation, which results in a substantial improvement of blood ejection. In addition, the actuators of the current design are positioned outside the cardiac chamber, which eliminates the risk of air embolism in case of an air leak from the actuator.

We acknowledge the limitations to these studies. We report an acute feasibility study in four animals because the main goal was to demonstrate proof of concept. In the preliminary RV study that uses ventricular pacing to cause HF, left heart function was also significantly impaired. For the timing and actuator contribution experiments, we only operated the device for a short period of time to observe relative changes at different operating parameters. This was done to prevent significant fluctuations in the HF baseline in between the trials. We could only operate the device at the heart rate of the animal during the in vivo studies, and it is likely that cardiac output varies for different heart rates. Last, we do not assess device biocompatibility or the long-term effects of device operation, because the primary objective of this work was to demonstrate feasibility of the approach. There is minimal blood contact with moving components in the proposed design, so it could potentially minimize thrombosis formation compared with existing therapies in current clinical practice.

In future work, we will perform in vivo studies to verify the longer-term biocompatibility, reliability, and performance efficacy of the device. We believe that future embodiments of the device could be fabricated from biocompatible materials commonly used in regulatory-approved blood-contacting devices such as intra-aortic balloon pumps, septal defect closure devices, and artificial valves. Biocompatible hydrogels that can be adhered to soft tissue may also be used as an interface between the soft actuators and ventricle surface (*47*). Emerging actuation technologies being developed within the soft robotics community pose exciting possibilities for soft robotic cardiac assist implants. The reliability of soft robotic VADs may be enhanced through the use of vacuum-based buckling actuators, which are inherently less prone to rupture (*48*). Foam-based soft actuators that can be sculpted into arbitrary shapes may allow improved conformability to the heart surface (*49*). Actuators with intrinsic sensing capabilities (*50*) may offer enhanced controllability of soft robotic VADs. A control system that triggers the VAD using the ventricular surface electrocardiogram signal will enable reliable device triggering over longer periods of time. In addition, blood pressure sensors integrated into the bracing assembly can be used for in situ blood pressure monitoring that will provide additional sensing redundancy for triggering device actuation without the need for an intracardiac catheter. Emerging soft sensor designs fabricated from biocompatible conductive hydrogels (*51*) may also be integrated into the actuators to enable strain and force monitoring for enhanced control of the soft robotic implant.

MATERIALS AND METHODS

Device fabrication

The soft actuator design was based on the McKibben pneumatic artificial muscle concept. A thermoplastic elastomer (TPE) bladder (Stretchlon 200, Airtech International) was fabricated using a heat press and former. A polyurethane airline was bonded to the base of the TPE bladder, and the entire assembly was then encapsulated within a mesh (diameter, 1 inch). We used a rubber outer skin on the actuator to enable rapid recoil back during diastole to promote refilling of the heart. The semilunar frame for the RV design was a turned aluminum disc to which the soft actuators were mechanically affixed. A separate implementation of the RV device was fabricated to incorporate force sensors (Honeywell model 11 subminiature load cell, Honeywell International) for brace force characterization. In the LV implementation, PolyJet 3D printing (Connex, Stratasys) was used to fabricate the semilunar frame. The brace bar was fabricated from polyether ether ketone (PEEK) to minimize the volume of metal to reduce noise artifacts during ultrasound imaging in vivo. The septal anchor and disc assemblies were produced from the PEEK and stainless steel to tolerate the dynamic mechanical loading during device operation. The RV device weighed 65.5 g, and the semilunar frame was 110 mm in diameter; the LV device weighed 38.7 g, and the semilunar brace was 90 mm in diameter.

Control system

A custom electropneumatic control system was developed to actuate the device. For the design embodiment intended for the RV, a pacemaker was used to simultaneously pace the native heart and provide an input to the control system. In the RV pressure overload and LHF experiments, we used a pressure-sensing catheter in the failing ventricle to detect the end of diastole and beginning of systole. The signal (pacemaker or ventricular pressure) was acquired through an analog input module (NI 9205, National Instruments) and processed by a real-time controller (cRIO-9030, National Instruments), which then generated output signals to trigger up to three pneumatic valves (NVKF333-5G-01T, SMC Corporation). The control system permitted the actuator valves to be opened for an arbitrary time period after detection of the input trigger. The software can also be configured to autonomously regulate the systolic actuation timing as a fixed fraction of the cardiac cycle according to the instantaneous heart rate. A host PC was used to communicate these timing variable values to the real-time system. The control box received an air pressure and vacuum supply, and the valves are configured to provide either vacuum or pressure to the actuators. A regulator (ITV series, SMC Corporation) was used to maintain the air pressure and was controlled by the real-time system. The host PC provided a graphical user interface of the instantaneous regulator pressure, trigger signal, and valve timing configuration.

Deployment procedure

The device was braced to the IVS through an anchoring system. Figure 3 and movie S2 illustrate the anchoring system and workflow for deployment on the failing RV, and access was simply reversed for deployment of the device on the LV. The anchor assembly was composed of a collapsible anchor intended for deployment on the healthy ventricle side of the septum (the LV according to Fig. 3). A rigid disc for the failing ventricle side (the RV according to Fig. 3) and anchor on the healthy ventricle side were connected together to create a "sandwich" around the septal tissue.

A purse string suture was placed at the access point, and access to the failing ventricle free wall and the IVS into the healthy ventricle was obtained using the Seldinger technique under echocardiography guidance. A guidewire was passed through the needle before the needle itself was removed from the ventricle (Fig. 3A). A series of dilators were passed over the guidewire so as to enlarge the septal tunnel to the healthy ventricle. Last, a 20-French dilator with the introducer sheath was inserted, and the dilator was removed to form a conduit to the healthy ventricle through which the anchor can be inserted. The collapsible anchor was composed of a threaded stud with four PEEK hinge elements. A nitinol spring couples the PEEK hinges of the anchor to each other, so the assembly was nominally in an expanded state but can be collapsed and passed through a sealed 20-French introducer sheath (Fig. 3B). The collapsible anchor was coupled to a detachable delivery shaft, and the anchor was primed into its collapsed state using a nitinol wire that was held in tension. When passed to the healthy ventricle, the nitinol wire tension was released, which allowed the PEEK hinges to spring open, and the anchor was pulled against the septum (Fig. 3C). The 20-French introducer sheath was removed, and a second sealed delivery tube was used to deploy the septal disc within the failing ventricle. The disc incorporated a threaded boss that was screwed onto the threaded stud of the collapsible anchor. The disc was retained onto the tip of the delivery tube using a Kevlar thread that was looped through holes in the disc and held in tension. The delivery tube was then passed over the anchor delivery shaft, through the failing ventricle free wall, before it was affixed to the septal anchor (Fig. 3D). The anchor delivery shaft was removed, and the bracing bar was passed through the delivery tube system and affixed to the septal disc. The bracing bar has a TPE sealing sleeve (Stretchlon 200, Airtech International) bonded at the distal region to prevent blood flow through the perforation made in the ventricle wall (see Fig 1, A and D). The delivery tube was removed, and the ventricle free wall tissue was pulled tight around the brace bar and sealing sleeve (Fig. 3E). A lipped ring was placed inside the sleeve, and the ventricle free wall purse string suture was released so that the ring can be inserted into the wall of the ventricle (Fig. 3F). The purse string suture was pulled taut once again to create a seal around the ring.

An adjustable clamping mechanism allows the orientation of the semilunar frame to be adjusted for optimal positioning of the actuators over the ventricle free wall. If the VAD is no longer required, the brace bar is disconnected from the septal anchor and withdrawn from the ventricle. The septal anchor is left inside the IVS, in a similar manner to catheter-based ventricular septal defect closure devices (*52*). In case VAD operation is required again, the brace bar can be introduced back inside the ventricle under echocardiography guidance and reconnected with the septal anchor, allowing reimplantation of the device.

In vivo testing

We performed nonsurvival in vivo studies in a porcine model (n = 4, ~75 kg). The 1996 *Guide for the Care and Use of Laboratory Animals* recommended by the U.S. National Institutes of Health was adhered to. We received ethical approval for the experimental protocol through the Institutional Animal Care and Use Committee and the study was performed at the Boston Children's Hospital. The pigs were put under general anesthesia, and mechanical ventilation was used throughout the study. Lidocaine was administered to minimize the risk of ventricular arrhythmias. Flow probes (16PS and 20PS, Transonics Corporation) were placed on the aorta and pulmonary artery. Pressure transducers (SurgiVet, Smiths Medical) were placed in the pulmonary artery, RV, and LV. The pressure transducer signals, surface electrocardiogram, and end-tidal CO_2 signals were passed to a clinical monitoring system (SurgiVet, Smiths Medical). A further signal from the device control system indicated the instantaneous state of the actuator control valve. The anchor and brace bar assembly was implanted using the procedure as previously outlined, on the beating heart. Standard dosing of heparin, which is used during intracardiac device deployment procedures (150 to 300 U/kg, activated clotting time above 250 s), was used during the deployment of the septal anchoring system and brace bar to minimize the risk of a thromboembolic event occurring. The semilunar frame with actuators was then affixed into position, and the airlines were connected to the control box.

For initial device characterization on the RV, we used pacing to create global HF. Although this HF model does not reflect RHF and adversely affects LV function, HF is easily reversible and provided a convenient means of safely characterizing the device. For the pressure overload RHF model, an inextensible band was placed around the main pulmonary artery. The band was tightened so as to reduce its circumference and constrict the pulmonary artery, initially by 5 mm and then by 10 mm to reduce pulmonary flow to around 50% of the healthy baseline. Actuators were inflated to 10 psi and for a systolic period equivalent to 35% of the total cardiac cycle. For the LV coronary ligation procedure, the diagonal branches of the left anterior descending artery and the obtuse marginal branches of the circumflex artery were ligated using sutures and tightened until aortic flow was reduced to around 50% of baseline. We actuated the device at 12 psi with a systolic actuation period of 40% of the cardiac cycle, with zero delay. For the microvasculature occlusion model of LHF, polystyrene microbeads of a nominal diameter of 50 to 100 μm (Megabead NIST, Polysciences Inc.) were injected into both the left anterior descending and the circumflex arteries to occlude the microvasculature of the LV free wall and the IVS. Actuators were inflated at 12 psi with a 40% systolic actuation period and with zero delay.

Data collection and statistical analysis

For all of the physiological conditions tested (baseline, HF, and device operation under different conditions), we logged individual volume ejections from the pulmonary artery and aorta, RV and LV pressures (systolic and diastolic), aortic pressure (systolic and diastolic). Pulmonary artery pressure (systolic and diastolic) and end-tidal CO_2 data were also logged in the RV experiments. All signals were then acquired by a data logging system (PowerLab, ADInstruments) at a rate of 1 kHz. The transducers were all calibrated, and a baseline measurement was taken. Ejection volumes for each cycle were computed by integrating the pulmonary artery and aortic flow rate data using analysis software (LabChart, ADInstruments). Individual pulmonary artery and aortic flow rates were computed for each cardiac cycle by multiplying the ejection volume by the instantaneous heart rate. Normality tests were performed on the data set using histograms. We performed a one-way analysis of variance (ANOVA) to determine statistical

significance with Tukey's post hoc test. We considered $P < 0.05$ to be statistically significant. For device characterization in the RHF pressure overload model and the LHF models, we considered $n = 15$ individual consecutive cardiac cycles. For the RV characterization study using ventricular pacing to create HF, we used $n = 10$ consecutive cycles for the timing characterization and actuator contribution studies. We considered $n = 15$ consecutive cycles for the brace force quantification experiment.

SUPPLEMENTARY MATERIALS

robotics.sciencemag.org/cgi/content/full/2/12/eaan6736/DC1
Materials and Methods
Fig. S1. Pressure-displacement characteristics of the actuators.
Fig. S2. Soft actuator contraction response times.
Fig. S3. Force characterization of a soft actuator at varying inflation pressure.
Fig. S4. Ex vivo testing on the RV.
Fig. S5. Plots showing forces applied to the RV in vivo and corresponding pulmonary flow rates.
Fig. S6. Characterization of the soft robotic device actuator on the RV in a pacing-induced HF after 5 min of continuous operation.
Movie S1. Device concept and ex vivo and in vivo footage.
Movie S2. Deployment procedure of the septal bracing system.
Movie S3. Demonstration of septal motion.

REFERENCES AND NOTES

1. D. Rus, M. T. Tolley, Design, fabrication and control of soft robots. *Nature* **521**, 467–475 (2015).
2. F. Ilievski, A. D. Mazzeo, R. F. Shepherd, X. Chen, G. M. Whitesides, Soft robotics for chemists. *Angew. Chem. Int. Ed. Engl.* **50**, 1890–1895 (2011).
3. R. F. Shepherd, F. Ilievski, W. Choi, S. A. Morin, A. A. Stokes, A. D. Mazzeo, X. Chen, M. Wang, G. M. Whitesides, Multigait soft robot. *Proc. Natl. Acad. Sci. U.S.A.* **108**, 20400–20403 (2011).
4. S. Kim, C. Laschi, B. Trimmer, Soft robotics: A bioinspired evolution in robotics. *Trends Biotechnol.* **31**, 287–294 (2013).
5. C. Laschi, B. Mazzolai, M. Cianchetti, Soft robotics: Technologies and systems pushing the boundaries of robot abilities. *Sci. Rob.* **1**, eaah3690 (2016).
6. D. P. Holland, E. J. Park, P. Polygerinos, G. J. Bennett, C. J. Walsh, The soft robotics toolkit: Shared resources for research and design. *Soft Rob.* **1**, 224–230 (2014).
7. E. T. Roche, R. Wohlfarth, J. T. Overvelde, N. V. Vasilyev, F. A. Pigula, D. J. Mooney, K. Bertoldi, C. J. Walsh, A bioinspired soft actuated material. *Adv. Mater.* **26**, 1200–1206 (2014).
8. F. Connolly, C. J. Walsh, K. Bertoldi, Automatic design of fiber-reinforced soft actuators for trajectory matching. *Proc. Natl. Acad. Sci. U.S.A.* **114**, 51–56 (2017).
9. S. Sareh, J. Rossiter, A. Conn, K. Drescher, R. E. Goldstein, Swimming like algae: Biomimetic soft artificial cilia. *J. R. Soc. Interface* **10**, 20120666 (2013).
10. B. Mazzolai, L. Margheri, M. Cianchetti, P. Dario, C. Laschi, Soft-robotic arm inspired by the octopus: II. From artificial requirements to innovative technological solutions. *Bioinspir. Biomim.* **7**, 025005 (2012).
11. H.-T. Lin, G. G. Leisk, B. Trimmer, GoQBot: A caterpillar-inspired soft-bodied rolling robot. *Bioinspir. Biomim.* **6**, 026007 (2011).
12. M. Cianchetti, T. Ranzani, G. Gerboni, T. Nanayakkara, K. Althoefer, P. Dasgupta, A. Menciassi, Soft robotics technologies to address shortcomings in today's minimally invasive surgery: The STIFF-FLOP approach. *Soft Rob.* **1**, 122–131 (2014).
13. A. Stilli, H. A. Wurdemann, K. Althoefer, Shrinkable, stiffness-controlled soft manipulator based on a bio-inspired antagonistic actuation principle, in *2014 IEEE/RSJ International Conference on Intelligent Robots and Systems*, (IEEE, 2014), pp. 2476–2481.
14. H. Rafii-Tari, C. J. Payne, G.-Z. Yang, Current and emerging robot-assisted endovascular catheterization technologies: A review. *Ann. Biomed. Eng.* **42**, 697–715 (2014).
15. P. Polygerinos, K. C. Galloway, E. Savage, M. Herman, K. O'Donnell, C. J. Walsh, Soft robotic glove for hand rehabilitation and task specific training, in *2015 IEEE International Conference on Robotics and Automation (ICRA)*, (IEEE, 2015), pp. 2913–2919.
16. P. Polygerinos, Z. Wang, K. C. Galloway, R. J. Wood, C. J. Walsh, Soft robotic glove for combined assistance and at-home rehabilitation. *Rob. Auton. Syst.* **73**, 135–143 (2015).
17. A. T. Asbeck, S. M. M. De Rossi, K. G. Holt, C. J. Walsh, A biologically inspired soft exosuit for walking assistance. *Int. J. Rob. Res.* **34**, 744–762 (2015).
18. B. T. Quinlivan, S. Lee, P. Malcolm, D. M. Rossi, M. Grimmer, C. Siviy, N. Karavas, D. Wagner, A. Asbeck, I. Galiana, C. J. Walsh, Assistance magnitude versus metabolic cost reductions for a tethered multiarticular soft exosuit. *Sci. Rob.* **2**, eaah4416 (2017).
19. F. A. Panizzolo, I. Galiana, A. T. Asbeck, C. Siviy, K. Schmidt, K. G. Holt, C. J. Walsh, A biologically-inspired multi-joint soft exosuit that can reduce the energy cost of loaded walking. *J. Neuroeng. Rehabil.* **13**, 43 (2016).
20. C. A. Cezar, E. T. Roche, H. H. Vandenburgh, G. N. Duda, C. J. Walsh, D. J. Mooney, Biologic-free mechanically induced muscle regeneration. *Proc. Natl. Acad. Sci. U.S.A.* **113**, 1534–1539 (2016).
21. E. T. Roche, M. A. Horvath, I. Wamala, A. Alazmani, S.-E. Song, W. Whyte, Z. Machaidze, C. J. Payne, J. C. Weaver, G. Fishbein, J. Kuebler, N. V. Vasilyev, D. J. Mooney, F. A. Pigula, C. J. Walsh, Soft robotic sleeve supports heart function. *Sci. Transl. Med.* **9**, eaaf3925 (2017).
22. C. J. Payne, I. Wamala, C. Abah, T. Thalhofer, M. Saeed, D. Bautista-Salinas, M. A. Horvath, N. V. Vasilyev, E. T. Roche, F. A. Pigula, C. J. Walsh, An implantable extracardiac soft robotic device for the failing heart: Mechanical coupling and synchronization. *Soft Rob.* **4**, 241–250 (2017).
23. E. Park, N. Mehandru, T. Lievano Beltran, E. Kraus, D. Holland, P. Polygerinos, N. V. Vasilyev, C. Walsh, An intraventricular soft robotic pulsatile assist device for right ventricular heart failure. *J. Med. Devices* **8**, 020908 (2014).
24. S. C. Obiajulu, E. T. Roche, F. A. Pigula, C. J. Walsh, Soft pneumatic artificial muscles with low threshold pressures for cardiac compression device, in *ASME 2013 International Design Engineering Technical Conferences and Computers and Information in Engineering Conference* (American Society of Mechanical Engineers, 2013), pp. V06AT07A009–V006AT007A009.
25. M. A. Horvath, I. Wamala, E. Rytkin, E. Doyle, C. J. Payne, T. Thalhofer, I. Berra, A. Solovyeva, M. Saeed, S. Hendren, E. T. Roche, P. J. Del Nido, C. J. Walsh, N. V. Vasilyev, An intracardiac soft robotic device for augmentation of blood ejection from the failing right ventricle. *Ann. Biomed. Eng.* **45**, 2222–2233 (2017).
26. B. C. Mac Murray, X. An, S. S. Robinson, I. M. van Meerbeek, K. W. O'Brien, H. Zhao, R. F. Shepherd, Poroelastic foams for simple fabrication of complex soft robots. *Adv. Mater.* **27**, 6334–6340 (2015).
27. Writing Group Members; D. Mozaffarian, E. J. Benjamin, A. S. Go, D. K. Arnett, M. J. Blaha, M. Cushman, S. R. Das, S. de Ferranti, J. P. Després, H. J. Fullerton, V. J. Howard, M. D. Huffman, C. R. Isasi, M. C. Jiménez, S. E. Judd, B. M. Kissela, J. H. Lichtman, L. D. Lisabeth, S. Liu, R. H. Mackey, D. J. Magid, D. K. McGuire, E. R. Mohler III, C. S. Moy, P. Muntner, M. E. Mussolino, K. Nasir, R. W. Neumar, G. Nichol, L. Palaniappan, D. K. Pandey, M. J. Reeves, C. J. Rodriguez, W. Rosamond, P. D. Sorlie, J. Stein, A. Towfighi, T. N. Turan, S. S. Virani, D. Woo, R. W. Yeh, M. B. Turner; American Heart Association Statistics Committee; Stroke Statistics Subcommittee, Heart disease and stroke statistics—2016 update: A report from the American Heart Association. *Circulation* **133**, e38–e360 (2016).
28. M. M. Givertz, Ventricular assist devices: Important information for patients and families. *Circulation* **124**, e305–e311 (2011).
29. L. E. Rodriguez, E. E. Suarez, M. Loebe, B. A. Bruckner, Ventricular assist devices (VAD) therapy: New technology, new hope? *Methodist Debakey Cardiovasc. J.* **9**, 32–37 (2013).
30. J. G. Rogers, F. D. Pagani, A. J. Tatooles, G. Bhat, M. S. Slaughter, E. J. Birks, S. W. Boyce, S. S. Najjar, V. Jeevanandam, A. S. Anderson, I. D. Gregoric, H. Mallidi, K. Leadley, K. D. Aaronson, O. H. Frazier, C. A. Milano, Intrapericardial left ventricular assist device for advanced heart failure. *N. Engl. J. Med.* **376**, 451–460 (2017).
31. J. A. Frontera, R. Starling, S.-M. Cho, A. S. Nowacki, K. Uchino, M. S. Hussain, M. Mountis, N. Moazami, Risk factors, mortality and timing of ischemic and hemorrhagic stroke with left ventricular assist devices. *J. Heart Lung Transplant.* **36**, 673–683 (2016).
32. J. Suarez, C. B. Patel, G. M. Felker, R. Becker, A. F. Hernandez, J. G. Rogers, Mechanisms of bleeding and approach to patients with axial-flow left ventricular assist devices. *Circ. Heart Fail.* **4**, 779–784 (2011).
33. X. Wang, A. L. Zachman, N. A. Haglund, S. Maltais, H. J. Sung, Combined usage of stem cells in end-stage heart failure therapies. *J. Cell. Biochem.* **115**, 1217–1224 (2014).
34. P. Janaswamy, T. E. Walters, B. Nazer, R. J. Lee, Current treatment strategies for heart failure: Role of device therapy and lv reconstruction. *Curr. Treat. Options Cardiovasc. Med.* **18**, 57 (2016).
35. M. H. Kwon, M. Cevasco, J. D. Schmitto, F. Y. Chen, Ventricular restraint therapy for heart failure: A review, summary of state of the art, and future directions. *J. Thorac. Cardiovasc. Surg.* **144**, 771–777.e1 (2012).
36. M. C. Oz, J. H. Artrip, D. Burkhoff, Direct cardiac compression devices. *J. Heart Lung Transplant.* **21**, 1049–1055 (2002).
37. L. A. Sánchez, C. E. Guerrero-Beltrán, A. M. Cordero-Reyes, G. García-Rivas, G. Torre-Amione, Use of stem cells in heart failure treatment: Where we stand and where we are going. *Methodist Debakey Cardiovasc. J.* **9**, 195–200 (2013).
38. M. Cevasco, M. Kwon, A. Fiedler, L. S. Lee, J. Shiao, R. V. Shah, A. H. Worthington, J. A. Fox, R. Y. Kwong, F. Y. Chen, Right heart failure: An ischemic model and restraint therapy for treatment. *Ann. Thorac. Surg.* **97**, 1356–1363 (2014).
39. G. D. Buckberg; RESTORE Group, The ventricular septum: The lion of right ventricular function, and its impact on right ventricular restoration. *Eur. J. Cardiothorac. Surg.* **29**, S272–S278 (2006).

40. F. Haddad, R. Doyle, D. J. Murphy, S. A. Hunt, Right ventricular function in cardiovascular disease, part II: Pathophysiology, clinical importance, and management of right ventricular failure. *Circulation* **117**, 1717–1731 (2008).
41. N. F. Voelkel, R. A. Quaife, L. A. Leinwand, R. J. Barst, M. D. McGoon, D. R. Meldrum, J. Dupuis, C. S. Long, L. J. Rubin, F. W. Smart, Y. J. Suzuki, M. Gladwin, E. M. Denholm, D. B. Gail; National Heart, Lung, and Blood Institute Working Group on Cellular and Molecular Mechanisms of Right Heart Failure, Right ventricular function and failure: Report of a National Heart, Lung, and Blood Institute working group on cellular and molecular mechanisms of right heart failure. *Circulation* **114**, 1883–1891 (2006).
42. N. C. Dang, V. K. Topkara, M. Mercando, J. Kay, K. H. Kruger, M. S. Aboodi, M. C. Oz, Y. Naka, Right heart failure after left ventricular assist device implantation in patients with chronic congestive heart failure. *J. Heart Lung Transplant.* **25**, 1–6 (2006).
43. G. Buckberg, J. I. E. Hoffman, Right ventricular architecture responsible for mechanical performance: Unifying role of ventricular septum. *J. Thorac. Cardiovasc. Surg.* **148**, 3166–3171. e4 (2014).
44. Y. Carrascal, A. L. Guerrero, Neurological damage related to cardiac surgery: Pathophysiology, diagnostic tools and prevention strategies. Using actual knowledge for planning the future. *Neurologist* **16**, 152–164 (2010).
45. L. J. Dell'Italia, Anatomy and physiology of the right ventricle. *Cardiol. Clin.* **30**, 167–187 (2012).
46. M. Morcos, F. H. Sheehan, Regional right ventricular wall motion in tetralogy of Fallot: A three dimensional analysis. *Int. J. Cardiovasc. Imaging* **29**, 1051–1058 (2013).
47. J. Li, A. D. Celiz, J. Yang, Q. Yang, I. Wamala, W. Whyte, B. R. Seo, N. V. Vasilyev, J. J. Vlassak, Z. Suo, D. J. Mooney, Tough adhesives for diverse wet surfaces. *Science* **357**, 378–381 (2017).
48. D. Yang, M. S. Verma, J.-H. So, B. Mosadegh, C. Keplinger, B. Lee, F. Khashai, E. Lossner, Z. Suo, G. M. Whitesides, Buckling pneumatic linear actuators inspired by muscle. *Adv. Mater. Technol.* **1**, 1600055 (2016).
49. A. Argiolas, B. C. Mac Murray, I. Van Meerbeek, J. Whitehead, E. Sinibaldi, B. Mazzolai, R. F. Shepherd, Sculpting soft machines. *Soft Rob.* **3**, 101–108 (2016).
50. S. S. Robinson, K. W. O'Brien, H. Zhao, B. N. Peele, C. M. Larson, B. C. Mac Murray, I. M. Van Meerbeek, S. N. Dunham, R. F. Shepherd, Integrated soft sensors and elastomeric actuators for tactile machines with kinesthetic sense. *Extreme Mech. Lett.* **5**, 47–53 (2015).
51. C. Keplinger, J.-Y. Sun, C. C. Foo, P. Rothemund, G. M. Whitesides, Z. Suo, Stretchable, transparent, ionic conductors. *Science* **341**, 984–987 (2013).
52. L. Yang, B.-C. Tai, L. W. Khin, S. C. Quek, A systematic review on the efficacy and safety of transcatheter device closure of ventricular septal defects (VSD). *J. Interv. Cardiol.* **27**, 260–272 (2014).

Acknowledgments: We thank N. Crilley, E. Pollock, D. Bolgen, and the Animal Research Children's Hospital team. In addition, we acknowledge the assistance of T. Blough, P. Machado, A. Meckes, J. Weaver, and the Wyss Institute machine shop with the device prototyping and D. Zurakowski for advice on the statistical analysis. **Funding:** This work was supported in part by the U.S. Department of Defense Congressionally Directed Medical Research Programs Discovery Award W81XWH-15-1-0248 (to N.V.V.), the Wyss Institute for Biologically Inspired Engineering, and the Harvard John A. Paulson School of Engineering and Applied Sciences. **Competing interests:** A patent application relating to the research presented in this manuscript was submitted on 24 June 2016, application number 62/354,196; N.V.V. and C.J.P. were the inventors. All other authors declare that they have no competing interests. **Data and materials availability:** All data needed to evaluate the paper are in the main text or in the supplementary materials. All requests for additional data and materials should be addressed to N.V.V. (nikolay.vasilyev@childrens.harvard.edu).

Submitted 18 May 2017
Accepted 30 October 2017
Published 22 November 2017
10.1126/scirobotics.aan6736

Citation: C. J. Payne, I. Wamala, D. Bautista-Salinas, M. Saeed, D. Van Story, T. Thalhofer, M. A. Horvath, C. Abah, P. J. del Nido, C. J. Walsh, N. V. Vasilyev, Soft robotic ventricular assist device with septal bracing for therapy of heart failure. *Sci. Robot.* **2**, eaan6736 (2017).

Science Robotics

Soft robotic ventricular assist device with septal bracing for therapy of heart failure

Christopher J. Payne, Isaac Wamala, Daniel Bautista-Salinas, Mossab Saeed, David Van Story, Thomas Thalhofer, Markus A. Horvath, Colette Abah, Pedro J. del Nido, Conor J. Walsh, and Nikolay V. Vasilyev

Sci. Robot. **2** (12), eaan6736. DOI: 10.1126/scirobotics.aan6736

Science Robotics (ISSN 2470-9476) is published by the American Association for the Advancement of Science. 1200 New York Avenue NW, Washington, DC 20005. The title *Science Robotics* is a registered trademark of AAAS.